Six-quark resonance structures in nucleon-nucleon scattering

Paul LaFrance and Earle L. Lomon
Center for Theoretical Physics, Laboratory for Nuclear Science and Department of Physics, Massachusetts Institute of Technology, Cambridge, Massachusetts 02139
(Received 26 February 1986)

The effects of short-range QCD models on two-hadron reactions are quantitatively predictable using R-matrix theory. Inelastic resonances are predicted in the two-nucleon S-state channels. The positions and magnitudes of these resonances are model sensitive but their widths, energy splitting, and inelastic modes are characteristic of the six-quark states (dibaryons). With a coupled-channel model for the two-baryon long-range wave function, the MIT bag model is found to be inconsistent with known phase shifts, but the cloudy bag model is consistent and predicts resonances near 2.7 GeV/c^2 mass. The observables have been calculated for pp and np scattering with reasonable assumptions about the background phases, and several are shown to have excitation function structures that are detectable.

I. INTRODUCTION

Multihadron phenomena at intermediate energies may be able to provide essential information about QCD dynamics. The asymptotic-freedom property of QCD predicts several features which have been verified in high-energy, inclusive, deep-inelastic scattering and jet production. Although lattice QCD calculations have been making some progress, comparison of experiment with nonperturbative properties of QCD (such as those relating to confinement) have had to rely on models. The meson and baryon spectrum data determine parameters of these models but is not enough to discriminate among the many "successful" bag models and constituent-quark potential models. In particular, single-hadron observables are volume phenomena that are not sensitive to the dynamical assumptions in the transition region between asymptotic freedom and confinement. Two-hadron reactions transit these regions and are sensitive to all aspects of QCD. To the extent that it is possible to predict these reactions on the basis of the short-range quark degrees of freedom and the long-range hadronic description, one can impose many more restrictions on the QCD models and ultimately on QCD itself. One of the clearest signals of the quark-gluon degrees of freedom that one may expect is a resonance whose properties are related to those degrees of freedom. It is customary that six-quark resonances in two-baryon reactions are called dibaryons. In this paper, we will discuss in some detail the low-lying, S-state dibaryons in the two-nucleon system.

In the bag models, a sudden transition between the asymptotically free and the confined regions is assumed. The equilibrium radius of the bag is the boundary between these regions. The physical hadrons may differ from this picture in having a transition region. Such a region, of about 10—20% of the transition radius, is indicated both by lattice QCD calculations[1] and instanton gas models.[2] The hadron properties would be insensitive to the existence of a transition thickness of $<20\%$ of the equilibrium radius, because the masses and magnetic moments are volume effects. The bag parameters allow the equilibrium radius to attain some effective transition radius for which the integrals over the interior are similar in the bag model as in the more complex physical case.

However, this transition region has important implications for multi-hadron systems. As is made evident in R-matrix theory, two-hadron reactions depend on the derivatives of the interior quark wave functions *at the boundary*. These values can change rapidly as one moves from the asymptotically free region into the transition region. Hence, it will be more accurate to use a matching boundary radius that is smaller than the equilibrium radius and thus may be expected to be in the region in which asymptotic freedom is a good approximation.

We also note that the existence of this transition region implies that, as a whole, hadron can be expected to have substantial multi-quark-antiquark-pair and multigluon components. These nonvalence components would be concentrated in the transition region and valence dominance would be interior to that. This invalidates some inferences from simple models of many-hadron systems, such as nuclear matter. For instance, estimates of quark exchange based on the valence picture may overestimate the effect. In general, these more complex configurations may account for the fact that nuclei at low energy behave as collections of nucleons, not as collections of quarks. The results of this paper indicate that the quark aspects may show up when energies are reached which allow the penetration of the valence region.

Even in the valence-quark region, a two-hadron system becomes a many-quark problem. In such a situation it is not surprising if some of the many-body techniques developed for nuclear problems are useful. Cluster-model or resonating-group methods have been applied,[3] as well as projection-operator[4] and R-matrix-related methods.[5—10] The simplicity of the R-matrix method, and its ability to quantitatively connect specific quark models with experimental consequences, are among the reasons for presenting some detailed results of this approach here. Perhaps the most important reason is that this approach allows

one, in first order, to deal with the complex region of confinement, and approach to confinement, directly in terms of hadronic field theory.

In Sec. II we present the R-matrix formalism and models used here. Section III discusses the f-matrix poles of these models in S-state nucleon-nucleon channels. The observable effects of the six-quark resonances are described in Sec. IV and we summarize conclusions in Sec. V.

II. FORMALISM

The R-matrix method[11] has many advantages in this regard in that it takes maximal advantage of the separation into the two spatial regions and relates the two-hadron S-matrix to the masses of quark-gluon excited states determined by the QCD model and the choice of separation radius.[5,12] The external scattering states $\Psi_{\rm II}^W(\mathbf{r}) = \phi_{N_1}\phi_{N_2}\psi^W(\mathbf{r})$, where W is the barycentric energy and $\mathbf{r}$ is the relative coordinate between the c.m.'s of the quark-cluster baryons N_1 and N_2, are expanded for $r<r_0$ in the $\Psi_{\rm I}^i(\mathbf{r}_\alpha)$ of the QCD model satisfying $\Psi_{\rm I}^i(r_\alpha=R_0)=0$ for $\alpha=1,N$, where the $\mathbf{r}_\alpha$ are the N individual quark or gluon coordinates. [Note that as we are dealing with partial waves we choose to use wave functions defined by the reduced one-dimensional equation and which behave as $\sin(Kr+\delta)$ asymptotically.] The choice of boundary condition, i.e., vanishing wave function rather than vanishing gradient (as in nuclear applications) or vanishing linear combination of wave function and gradient, is suggested by the confinement property. R_0 is not a specific dynamical surface, but is a fixed boundary which must be chosen so that the applicable Hamiltonians $H_{\rm I}$ and $H_{\rm II}$ are good approximations to the physics in each region.[12] The standard R-matrix formalism does not prescribe explicit procedures for taking into account the different number of degrees of freedom and the different types of wave function (Dirac versus Schrödinger) in the interior and exterior regions. After averaging over the extra degrees of freedom, one can show in the approximation of free wave functions[5] that the effective internucleon boundary coordinate for which the interior wave function vanishes is

$$r_0 = 1.37[(n_1+n_2)/n_1n_2]^{1/2}R_0 \ ,$$

where n_1 and n_2 are the number of quarks in each hadron and R_0 is the bag-model radius.

R-matrix theory[11] uses continuity and Green's theorem to relate the overlap integral to the boundary condition on the external wave function

$$r_0\frac{d\psi_\alpha^W}{dr_0} = \sum_\beta f_{\alpha\beta}\psi_\beta^W(r_0) \tag{1}$$

with[5,8]

$$f_{\alpha\beta}(W) = f_{\alpha\beta}^0 + \sum_i \frac{\rho_{\alpha\beta}^i}{W-W_i} \ , \tag{2}$$

where W_i is the energy of the internal states Ψ^i and

$$\rho_{\alpha\beta}^i = \frac{r_0}{2m_r}(\Psi_{\rm I\alpha}^{*i'}\Psi_{\rm I\beta}^{i'})_{R_0} = -r_0\frac{\partial W_i}{\partial r_0}\xi_\alpha^i\xi_\beta^i \ . \tag{3}$$

In the above equations, the multichannel aspect of the two-hadron wave function is made explicit by the α,β subscripts and the ξ_α^i are the fractional parentage coefficients of channel α in the internal state i. The second form of Eq. (3) was derived in Ref. 5. Both forms make manifest the positivity of the residues, which was shown in Ref. 12 to follow from causality. The important relation $df_{\alpha\beta}/dW \le 0$ follows, where the upper limit corresponds to a constant f matrix and implies maximum nonlocality within r_0. This is a statement of the Wigner causality condition $d\delta/dk \ge -r_0$ which, in the original form, is only valid when the interaction vanishes for $r>r_0$.

We note that the constant term $f_{\alpha\beta}^0$ is not determined by the internal states and in practice also approximately represents all pole terms for $i>N$, where $\Psi_{\rm I}^N$ is the last state explicitly represented and $W \ll W_{N+1}$.

In this application we use various bag models for $H_{\rm I}$ so that the $\psi_{\rm I}^i$ are antisymmetrized products of the free-quark wave functions which vanish at R_0. Including one-gluon-exchange terms and the difference of the perturbative and physical vacuum energy densities, $H_{\rm I}$ is represented[8] by its expectation value[5,13]

$$H_{\rm I}(n,R) = R^{-1}A(n) + \tfrac{4}{3}\pi BR^3 + \tfrac{4}{3}\pi B(R_T^3-R^3)\Lambda_0\theta(R-R_T) \ , \tag{4}$$

where $A(n)=nE_q(mR)-Z_0+\alpha_s\Delta E_m$, with ΔE_m giving the color-magnetic splitting due to single-gluon exchange, Z_0 representing gluonic vacuum fluctuations in a cavity (and sometimes c.m. motion effects), and the single-quark energy is, for massless ${}^1S_{1/2}$ quarks, $E_q(0)=2.04-\alpha_s e$, e representing the quark self-energy in a cavity.[14] The last term[5] is needed in exotic systems in which it is energetically favorable for the two color-singlet clusters (for which Λ_0 is the projection operator) to separate into two bags for $R>R_T$ (the transition radius $R_T \ge R_{\rm eq}$ the equilibrium radius). That term is essential in the R-matrix application of Refs. 5 and 6 in which $R_0=R_{\rm eq}$ is used. However, we argue[8] that it is necessary to choose $R_0<R_{\rm eq}$, as the residues are sensitive to the wave functions at the surface [Eq. (3)]. $R_{\rm eq}$ is in the middle of the transition region to confinement so that the assumption of asymptotic freedom is not valid at $R_{\rm eq}$. Lattice QCD calculations[1] indicate that asymptotic freedom sets in strongly at $R \approx (0.8\text{–}0.9)R_{\rm eq}$. Indeed, if asymptotic freedom is not valid at $R \approx 0.8R_{\rm eq}$ then asymptotic freedom would apply to half or less of the volume of a hadron and the success of bag models for hadrons must be considered accidental. We therefore expect $0.8R_{\rm eq}<R_0<R_{\rm eq}$. A substantial transition region implies that the valence-quark dominance assumed by current models is inadequate.

For the exterior region $H_{\rm II}$ is taken to be the Feshbach-Lomon potential[15] derived from π, 2π, η, ρ, and ω exchange in the two-nucleon sector, and is connected to the $N\Delta$, $\Delta\Delta$, and $NN^*(1440)$ sectors[16] by one-pion exchange and sometimes by phenomenological two-pion range potentials $V_{\rm trans}^{2\pi}$. It has been shown[16,17] that such a coupled-channel system fits the data for $W \le 2.3$ GeV well with a *constant* f matrix when the boundary is chosen at $r_0 \approx \frac{1}{2}m_\pi^{-1}$. This implies that for this radius,

f poles are all at substantially higher W, which is certainly true for the MIT (Ref. 13) and cloudy[18] bag models.

If the dominance of asymptotic freedom in the interior requires $R_0 < R_{eq}$, then is a clustered hadronic model adequate for $r > r_0$? It has been shown[19] that the potential derived from hadronic field theory using dispersion relations,[20] involving no free parameters or any reference to the quark and gluon degrees of freedom, is, for $r \gtrsim 0.9$ fm, in agreement with the accurate NN data up to energies exceeding the pion production threshold. Other potentials invoking only meson exchange[8,15,21] for $r_0 \gtrsim 0.7$ fm have similar success. In addition to this *a posteriori* evidence, one may conjecture that hadronic clustering takes place to a sufficient extent very soon after higher-order QCD effects become substantial. This is indeed analogous to what happens in the shell model, where relatively small particle-hole corrections produce α clustering in the nuclear surface.

We note that the poles of the f matrix [Eq. (2)] become manifest in the hadron-hadron elastic-scattering channel as poles in an effective f matrix, $f_{\rm eff}$, which is obtained after eliminating the coupled isobar channels.[8,22] Because of the coupling, the poles of $f_{\rm eff}$ are slightly displaced[8] below the poles of f. To illustrate with a two-channel case, in channel 1

$$f_{\rm eff}(W) = f_{11} - (f_{12})^2 [f_{22} + \theta_2(W)]^{-1} , \tag{5}$$

where $\theta_2(W)$ is the logarithmic derivative of the outgoing wave function in channel 2. In the absence of a diagonal potential in channel 2 and if $L_2 = 0$

$$\theta_2(W) = -iK_2(W) r_0 \tag{6}$$

with $K_2(W)$ being the relative momentum in channel 2. If the f_{ij} components are now obtained from Eq. (2), keeping only a single internal eigenstate W_i, then

$$f_{\rm eff}(W) = f^0_{11} + (W - W_i)^{-1} \left[\rho_{11} + \frac{(f^0_{12})^2 (W - W_i)^2 + 2 f^0_{12} \rho_{12} (W - W_i) + \rho_{12}{}^2}{\rho_{22} + [f^0_{22} + \theta_2(W)](W - W_i)} \right] . \tag{7}$$

Expanding the above expression into its simple poles we have

$$f_{\rm eff}(W) = f^0_{11} - (f^0_{12})^2 [f^0_{22} + \theta_2(W)]^{-1} + (\rho_{11} - \rho_{12}{}^2 \rho_{22}{}^{-1})(W - W_i)^{-1} + \left[W - W_i + \frac{\rho_{22}}{[f^0_{22} + \theta_2(W)]} \right]^{-1} \left[\frac{(f^0_{12})^2 \rho_{22}}{[f^0_{22} + \theta_2(W)]^2} - \frac{2 f^0_{12} \rho_{12}}{[f^0_{22} + \theta_2(W)]} + \frac{\rho_{12}{}^2}{\rho_{22}} \right] . \tag{8}$$

The pole at $W = W_i$ vanishes because the factorizability of $\rho_{\alpha\beta}$ [see Eq. (3)] implies $\rho_{11}\rho_{22} = \rho_{12}{}^2$. This relation also simplifies the last term in the last set of large parentheses of Eq. (8) to ρ_{11}. Therefore, the pole at W_i is shifted to (ignoring the slow W dependence of θ_2)

$$W_p = W_i - \rho_{22} / \hat{f}^0_{22} \tag{9}$$

with residue

$$\rho_p = \rho_{22}{}^{-1} (\rho_{22} f^0_{12} / \hat{f}^0_{22} - \rho_{12})^2 \tag{10}$$

and

$$\hat{f}^0_{22} = f^0_{22} + \theta_2(W_i) .$$

Because of the general properties[22] of $\theta_2(W)$, as in the special case of Eq. (6), W_p is real and ρ_p is positive for $W_i \le W_{T2}$, the threshold energy for producing channel 2. For $W_i > W_{T2}$ they are complex as channel 1 is no longer conserved.

The R-matrix theory also allows one to calculate a quantity of theoretical interest: the probability of the system to be in the interior, free-quark region,[9]

$$P_{fq} \equiv \int_0^{r_0} \psi^\dagger(r) \psi(r)\, dr = -\frac{1}{r_0} \psi^\dagger(r_0) \frac{df}{d(K^2)} \psi(r_0) \tag{11}$$

$$= \sum_i \frac{2}{W r_0} (W - W_i)^{-2} \psi^\dagger(r_0) \rho_i \psi(r_0) , \tag{11a}$$

where Eq. (11a) applies for equal mass M particles in the incoming channel. The above form only has the meaning of a probability for discrete states. In the continuum, the wave function is not square integrable and we normalize to unit incoming flux, defining

$$I_{fq} \equiv \frac{M}{K} \int_0^{r_0} \psi^\dagger(r) \psi(r) dr \tag{12}$$

which differs from P_{fq} only by the factor M/K.

We note that at the poles, the right-hand side of Eqs. (11) and (11a) are only defined in the limit as $\psi(r_0)$ vanishes and $df/d(K^2)$ is infinite at that point. This also implies that near a pole only that pole contributes, and a one-pole approximation is adequate.

III. f POLES IN NN CHANNELS

We now find, for each bag model and each NN channel, the value of r_0 which satisfies the requirement that the lowest W_i for that channel is equal to the energy of the lowest f pole. The latter is found by integrating the wave function, fixed asymptotically by the experimental S matrix, from large r to r_0. By Eq. (1) there is an f pole at r_0 if $\Psi^W_{\rm II}(r_0) = 0$. Figure 1 shows the trajectories of the W_i and of the f poles for the bag models of Refs. 13, 14, and 18, for the $^1S_0$ and $^3S_1$-$^3D_1$ NN channels (coupled to isobar channels). The crossing of a W_i trajectory with the appropriate f-pole trajectory (or an extrapolation of it)

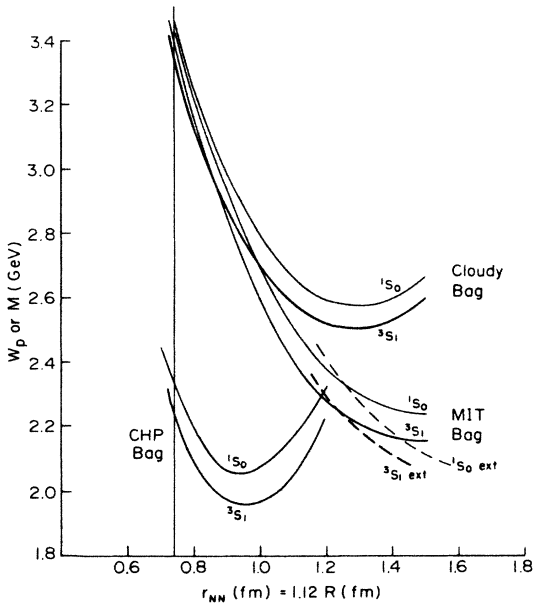

FIG. 1. Bag state energies for three different QCD models (solid curves) and experimental f-matrix pole energies (dashed curves) as a function of relative radius for the $NN(^1S_0)$ and $NN(^3S_1)$ channel models.

determines an r_0 consistent with the data. It then remains to be seen if the f-pole residue required by Eq. (3) is compatible with the data for any adjustment of the constant f^0 matrix (and sometimes a variation of the $V_{\text{trans}}^{2\pi}$). If so, the model will then predict consequences at higher energies.

It is important to note that for the $(^1S_{1/2})^6$ quark configurations $(\xi_{NN(S)})^2=\frac{1}{9}$ and $(\xi_{\Delta\Delta(S)})^2=\frac{4}{45}$ while all other nonvanishing ξ's are to hidden-color states. From Eq. (3) it follows that residues are small, producing resonant structures, dibaryons, near W_i. As the W_i are well above the elastic threshold for physically interesting cases, the resonances are very inelastic. Consequently, their effects are relatively small and are largely produced in the inelasticity parameter.

For the MIT bag model[13] (in which $e=0$ and c.m. recoil effects are only implicit in Z_0) the crossovers for both S-state channels (Fig. 1) are at $r_0=1.25$ fm or $R_0=1.12$ fm. Our bounds on R_0 are satisfied because $R_{\text{eq}}=1.3$ fm. The nonvanishing residue elements are ~ 0.12 GeV, and $W_i(^3S_1)=2.28$ GeV and $W_i(^1S_0)=2.34$ GeV. For this case there is *no* adjustment of the parameters f^0 and $V_{\text{trans}}^{2\pi}$ which produces a good fit to the experimental phase shifts for $W<2.3$ GeV. It is not the pole at the top of the experimental region which is the main obstacle to a fit because, due to the small residue, f is nearly constant over that region. It is the nearly constant f which at such a large r_0 causes too steep a decline in the phase shifts $(d\delta/dk\approx -r_0)$ (Ref. 12). Only by quadrupling the residues over the theoretical values [Eq. (3)] can one modify the f behavior in the experimental region sufficiently to fit the data. We conclude that the MIT bag model is not simultaneously compatible with the single-hadron and two-nucleon spectra.

We note that for $R_0=R_{\text{eq}}$ the situation is worse. The $^3S_1$ and $^1S_0$ $W_i=2.13$ and 2.16 GeV, respectively. This is in the experimentally determined region and, with the larger r_0, the residues have to be six times larger than the theoretical values to fit the data.[23] In any case one does not expect Eq. (3) to work in the transition region. In fact, in the meson-meson and meson-baryon sectors, where the relationship of f poles and the W_i is rather good, the residues need to be 20—100% larger than the theoretical values when one chooses $R_0=R_{\text{eq}}$ (Refs. 5 and 6).

In the CHP bag model (Ref. 14), $Z_0=0$, and approximate c.m. recoil corrections are applied to fit the hadron spectrum. The quark self-energy e is required by the hadron spectrum to be large and attractive. In the six-quark system this leads [see Eq. (4)] to a collapse to a small radius $R_{\text{eq}}=0.84$ fm, at low masses $W(^3S_1)=1.95$ GeV and $W(^1S_0)=2.05$ GeV as shown in Fig. 1. As the CHP parameters are determined after explicitly subtracting c.m. recoil corrections, that should also be done here. That would further lower the energy. This implies resonances in the well-studied low-energy region and is strongly inconsistent with the data.

In the cloudy bag model,[18] compression of the radius is a result of the pion cloud pressure and the masses are increased. Extrapolation of the experimental f-pole trajectories (Fig. 1) indicates a crossover at $R_0=0.9$ fm which is again about 20% less than R_{eq}, and predicts $W(^3S_1)=2.64$ GeV and $W(^1S_0)=2.71$ GeV. The nonvanishing theoretical residues are between S-wave states, $\rho_{NN,NN}=149.0$ MeV, $\rho_{NN,\Delta\Delta}=133.0$ MeV, and $\rho_{\Delta\Delta,\Delta\Delta}=118.718$ MeV. With these pole terms the f^0 for the $^1S_0$ and $^3S_1$-$^3D_1$ states can be adjusted to fit the $^1S_0$ and the $^3S_1$-$^3D_1$ phase parameters for $T_L\leq 1$ GeV. Strong f^0 coupling is required by the data, and in the $^3S_1$-$^3D_1$ case, the resulting energy dependence of ϵ_1 has more curvature than indicated by the present phase-shift analyses. Also, for elastic eD scattering the size of the core produces a diffraction minimum in the magnetic form factor at too small a momentum transfer,[24] requiring larger than expected meson-exchange current corrections at $q^2\sim 30$ fm^{-2}. This indicates that the cloudy-bag-model dynamics may not be fully adequate for the two-baryon system. A QCD model compatible with a somewhat smaller R_0 (for instance, one with a small attractive e in addition to Z_0) would fit the low-energy data more readily. However, small changes in the model do not change the residues much, so that the behavior of the observables predicted by the cloudy bag model will be typical of what may be expected. Below we present the results of this model and will point out which predictions are insensitive to the model (therefore acting as signatures of the six-quark system) and which are sensitive (therefore discriminating between models).

In Fig. 2 and Figs. 3 and 4 we show the behavior of the $^1S_0$ and the $^3S_1$-$^3D_1$ (for two different models) phase parameters, respectively, in the vicinity of the six-quark resonances. For the tensor coupled S matrix we use the representation

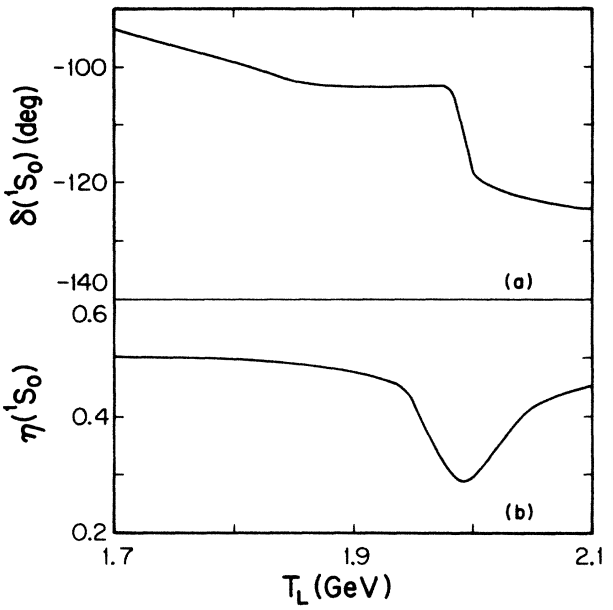

FIG. 2. The (a) phase shift δ and (b) inelasticity η, for the $NN(^1S_0)$ channel coupled to the $N\Delta(^5D_0)$, $\Delta\Delta(^1S_0)$, and $NN^*(1440)(^1S_0)$ channels and to the $[q(^1S_{1/2})]^6$ configuration of the cloudy bag model. Here, $f_{NN,NN}=18.25$, $f_{NN,N\Delta}=0.1$, $f_{NN,\Delta\Delta}=7.43$, $f_{NN,NN^*}=-7.43$, $f_{N\Delta,N\Delta}=1.5$, $f_{N\Delta,\Delta\Delta}=f_{N\Delta,NN^*}=f_{\Delta\Delta,NN^*}=0.0$, $f_{\Delta\Delta,\Delta\Delta}=3.0$, and $f_{NN^*,NN^*}=2.4$, are adjusted to fit the data for $T_L \leq 800$ MeV. Isobar widths are neglected.

$$S(^3S_1\text{-}^3D_1)=\begin{bmatrix} \eta_0 e^{2i\delta_0} & iA_1 \\ iA_1 & \eta_2 e^{2i\delta_2} \end{bmatrix},$$

where $A_1=\sin 2\epsilon_1 \exp[i(\delta_0+\delta_2+\phi_1)]$. The $^1S_0$ resonance is centered at $T_L=2.00$ GeV and the $^3S_1$-$^3D_1$ at $T_L=1.82$ GeV. The coupled-channel effect [see Eq. (9)] has moved the resonances down ~ 35 MeV from the f-pole positions. The width of the structures are ~ 50 MeV (c.m.). The energy spacing between these two structures of 70 MeV (c.m.) is very insensitive to the model because α_s is determined by N-Δ splitting in each model.

That the structure in the phase parameters is correlated with the penetration of the free six-quark region can be seen in Fig. 5 which is based on Eqs. (12) and (11). Also shown is the I_{fq} that would be obtained in the absence of interaction

$$I_{fq}(\text{free})=\frac{M}{K}\int_0^{r_0}\sin^2 Kr\,dr\ . \tag{13}$$

We note that the mismatch of the two-nucleon with the free six-quark wave function excludes all but a small fraction of the wave function from the interior, except in the vicinity of the resonance. At resonance, the wave function penetrates the interior so that the resonance properties are determined by the free-quark wave functions. As noted following Eq. (12), our one-state approximation to I_{fq} is accurate at the resonance. Away from the resonance the higher poles can contribute. Far below the resonance, near elastic threshold, the one-state result shown in Fig. 5 may strongly underestimate the penetration of the free-quark core.

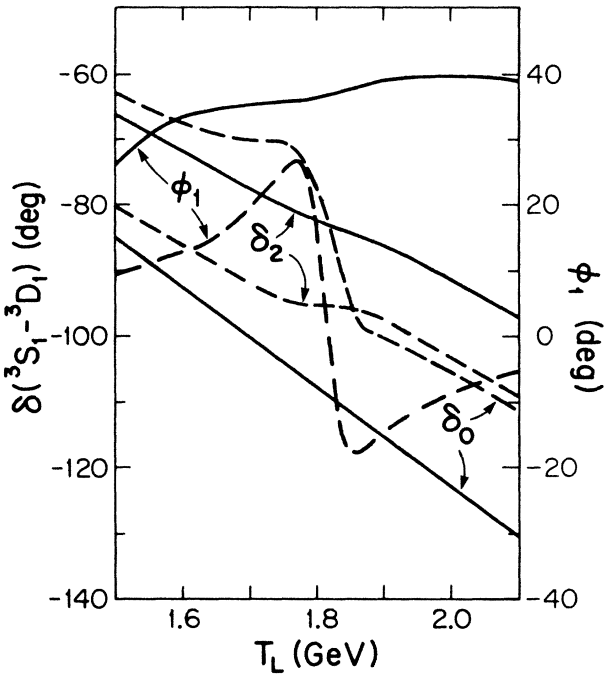

FIG. 3. The phase shifts δ_0, δ_2 and the imaginary coupling angle ϕ_1 for the $NN(^3S_1\text{-}^3D_1)$ channels coupled to the $\Delta\Delta(^3S_1)$, $\Delta\Delta(^7D_1)$, and $NN^*(^3S_1)$ channels and to the six-quark configuration. The dashed curves correspond to the model of Ref. 8 with quark coupling. The solid curves represent the model where $f_{S,S}=47.1028$, $f_{S,D}=-4.4$, $f_{S,\Delta\Delta(D)}=f_{S,\Delta\Delta(S)}=0.0$, $f_{S,NN^*}=-11.6$, $f_{D,D}=2.6$, $f_{D,\Delta\Delta(D)}=f_{D,\Delta\Delta(S)}=0.0$, $f_{D,NN^*}=-1.05$, $f_{\Delta\Delta(D),\Delta\Delta(D)}=2.5$, $f_{\Delta\Delta(D),\Delta\Delta(S)}=f_{\Delta\Delta(D),NN^*}=0.0$, $f_{\Delta\Delta(S),\Delta\Delta(S)}=0.3$, $f_{\Delta\Delta(S),NN^*}=0.0$, and $f_{NN^*,NN^*}=1.0$, are adjusted to fit the data for $T_L \leq 800$ MeV. Isobar widths are neglected in both cases.

The fractional parentage coefficients are model independent. Consequently, comparison of the widely different cases examined above shows that the resonance widths differ little from 50 MeV, several times smaller than expected from conventional resonance mechanisms (such as coupled-channel effects) in this energy range. The widths and energy splitting are therefore useful signatures of the appearance of $(^1S_{1/2})^6$ quark degrees of freedom.

The other good signatures are in the pion production channels due to $\Delta\Delta$ (S) states in the resonance region. Only the S-state NN and $\Delta\Delta$ color-singlet channels exist in the $(^1S_{1/2})^6$ quark configuration and the production of the latter varies rapidly throughout the resonance. The $\Delta\Delta$ production from the $^1S_0$ channel is shown in Refs. 9 and 10. This effect can be observed through the total two-pion production cross section, charge-state ratios, pion-nucleon angular correlations, and final-state nucleon spins. Figure 6 shows the $\Delta\Delta$ production from the $^3S_1$ and $^3D_1$ channels for both $^3S_1$-$^3D_1$ cases. The dip is caused by interference between the positive $f^0_{NN,\Delta\Delta}$ and the

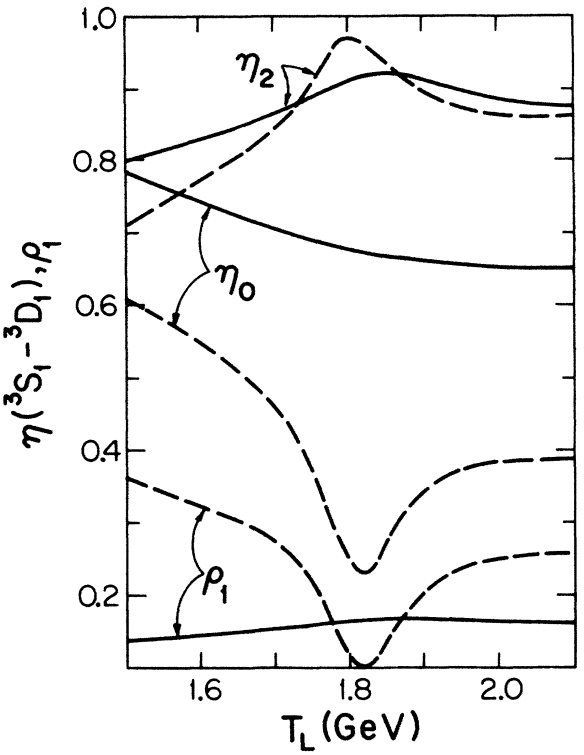

FIG. 4. The inelasticities η_0, η_2 and NN coupling strength $\rho_1=\sin 2\epsilon_1$, for the two $NN(^3S_1\text{-}^3D_1)$ coupled-channel systems described in Fig. 3.

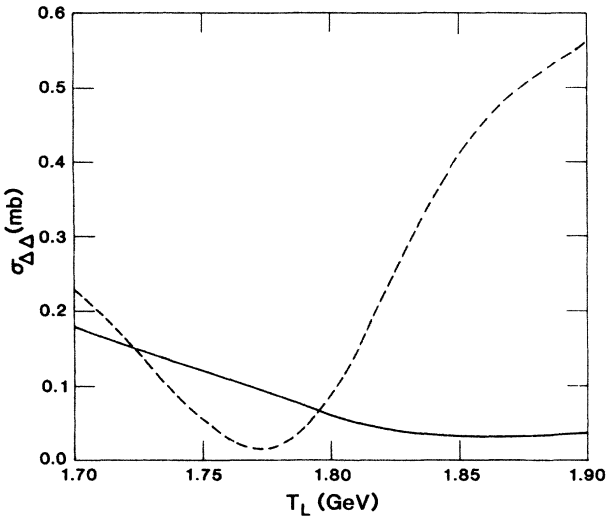

FIG. 6. The $\Delta\Delta$ production cross section from the $^3S_1$ and $^3D_1$ channels. The solid and dashed curves correspond to the two $^3S_1$-$^3D_1$ models of Figs. 3 and 4. Cross sections for production of specific $\pi\pi NN$ final states can be obtained by multiplying $\sigma_{\Delta\Delta}$ by appropriate Clebsch-Gordan coefficients.

pole term. Other mechanisms for producing a resonance would not be likely to lead to this $\Delta\Delta$ dominance. (Outside the resonance the $^1S_0$ inelasticity is expected to be dominated by one-pion production from the $N\Delta$ channel.)

The features of these dibaryonic resonances which are sensitive to the model are the absolute position of the energy and the amplitude of the observable effects. The position depends on specifics of the QCD model of the interior, such as coupling to the pion field, the inclusion of quark self-energy, and the radius within which asymptotic freedom is quantitatively adequate. Nevertheless, there are energy bounds within which one may expect these lower six-quark resonances to occur. Experience[15,16] has shown that for $R_0<0.7$ fm it is difficult to satisfy the Wigner causality condition $df/dW\leq 0$ with meson-exchange potentials, and that the data can be satisfied with constant f^0 (implying that poles are well above the experimental region). It follows from the lower bound on R_0 and Fig. 1 that the S-state resonances are expected to occur for $2.4<W<3.4$ GeV, within the range of present high current proton accelerators.

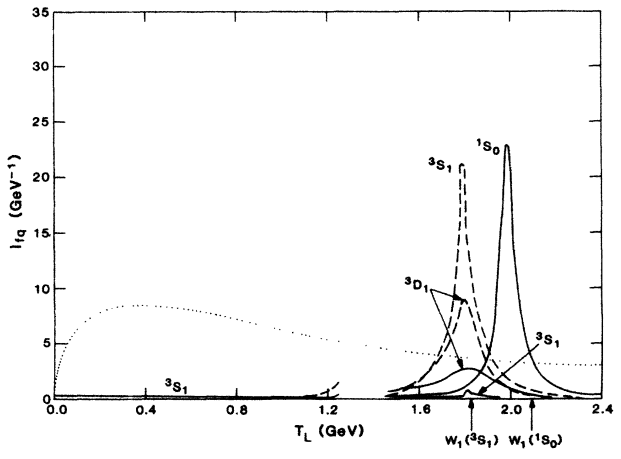

FIG. 5. The free-quark content of the $NN(^1S_0)$ and $NN(^3S_1\text{-}^3D_1)$ coupled-channel systems as determined by the cloudy-bag dynamics for the model of Fig. 2 and for the two models described in Figs. 3 and 4 (solid curves and dashed curves), respectively. The dotted curve represents I_{fq} of free nucleon-nucleon wave functions. The curves are not drawn in the vicinity of the $\Delta\Delta$ threshold because the calculation did not include the effect of the Δ decay width.

IV. *NN* OBSERVABLES AND THE SIX-QUARK RESONANCES

It is our present purpose to give guidance to the experimenter with respect to those observables in elastic nucleon-nucleon scattering which are most sensitive to the six-quark resonance effects. We do so using the above cloudy-bag-model $^1S_0$ and $^3S_1$-$^3D_1$ phases, and background phases of Refs. 16 and 17 to predict all the observables which have been experimentally studied at medium energies. The sensitivity of these assumptions is discussed below.

The amplitude of the observable effects depends on the background phases and therefore on the external interaction and the f^0. The variation of f due to the pole term is *not* very model dependent, as the residues are chiefly determined by the fractional parentage coefficients. But the effect of this variation on the resonant phase shift de-

pends on the background. If the background is very repulsive a fixed variation of f causes much less effect than if the background is attractive, because coupling to the interior is smaller in the first case. Also, the effect on an observable of a given variation of the resonant phase depends on the value of the nonresonant phases with which it interferes. We will demonstrate by example this variation in observable results. Because all the background phases must be extrapolated from $T_L = 0.8$ GeV by a model, this is the worst obstacle to predicting the ease or difficulty of observing these exotic six-quark resonance effects.

Figure 2 shows that both $\delta(^1S_0)$ and $\eta(^1S_0)$, from the fit to the $T_L \leq 800$ MeV data with a cloudy-bag-model interior, have substantial variation in the $^1S_0$ six-quark resonance region. In the case of the new $^3S_1$-$^3D_1$ waves of Figs. 3 and 4, however, the model that fits the scattering data reasonably well for $T_L \leq 800$ MeV, produces a resonantlike structure only in the inelasticity η_2 at the $^3S_1$ six-quark state. The observable consequences are then expected to be smaller than at the $^1S_0$ six-quark resonance. The other $I=0$ and $I=1$ background partial waves used are extrapolations to intermediate energies by a realistic coupled-channel model consistent with available data for $T_L \leq 800$ MeV, as described in Refs. 16 and 17. These phases are generally good fits to some phase-shift analyses and give a good description of the observables in this range of energies. Indeed, the values of $\sigma_{\rm tot}$, $\Delta\sigma_L$, and $\Delta\sigma_T$ reconstructed from this global model agree well with those from Arndt's *np* phase-shift solution for $T_L \leq 800$ MeV (Ref. 25). The smooth extrapolations constitute then a reasonable assumption on the background at higher energies.

The model for the $^3P_0$ wave is still the one of Ref. 16. Indeed, an analysis modified to include the two-pion decay of the $N^*(1440)$ half of the time, as treated in Ref. 17, is required only for $T_L \leq 1$ GeV. Beyond this energy, the average decay as it is now computed, yields the same results for δ and η as the one-pion decay analysis. The old $^3S_1$-$^3D_1$ model[8] has been corrected, for it yielded a wrong sign of ϵ_1. Extrapolation for this model including the f pole is shown in Figs. 3 and 4. The $^1S_0$ model used here could lead to values of the *NN* two-pion production cross section which are too big when compared with experimental ones. This is due to the large coupling parameters $f_{NN,\Delta\Delta} = -f_{NN,NN^*} = 7.43$ which should be lowered significantly (at the expense of increasing $f_{NN,N\Delta}$) in a future fine-tuning of the $^1S_0$ couplings.[26,27] In the *pp* case the model used for the $^3F_3$ wave is the one of Ref. 17.

The calculated observables in the laboratory frame belong to the set of zero-, one-, and two-spin index experiments; namely, the differential cross section $d\sigma/d\Omega$,the polarization P, the "diagonal" experiments $D(\equiv D_{n0n0} \equiv D_{NN}$ in the Saclay-Geneva and Argonne notation, respectively), D_t $(\equiv K_{n00n} \equiv K_{NN})$, A_{YY} $(\equiv C_{nn00} \equiv A_{NN})$, the analyzing powers A_{XX} $(\equiv A_{00ss} \equiv A_{SS})$, $-A_{ZX}$ $(\equiv A_{00sk} \equiv -A_{LS})$, and A_{ZZ} $(\equiv A_{00kk} \equiv A_{LL})$, and the Wolfenstein parameters A $(\equiv D_{s'0k0} \equiv D_{LS})$, A' $(\equiv D_{k'0k0} \equiv D_{LL})$, R $(\equiv D_{s'0s0} \equiv D_{SS})$, and R' $(\equiv D_{k'0s0} \equiv D_{SL})$. The Wolfenstein parameters in the Saclay-Geneva notation are expressed in terms of the tensor D_{a0c0}, rather than D_{0b0d}, because in those experiments, a polarized proton beam is scattered from a deuterium target and the scattered proton polarization is analyzed. The entire set of such lower-order polarization tensors is indeed the only one needed for a complete reconstruction of the scattering matrix (with no ambiguities, even discrete).[28] As a sample of the obtained angular distributions, Fig. 7 shows the spin correlation observable A_{XX} as a function of angle for three energies near the $^1S_0$ resonance in the *np* system. A typical example of a structure can be seen near 84° for instance, and illustrates the fact that energy structures occur over substantial angular intervals (here between 80° and 85°). Angular distributions for all the observables have been computed. We present here the excitation curves for each of the above *np* observables at those angles which are most sensitive to the resonances.

The observable consequences of the $^1S_0$ resonance in the *pp* system were discussed previously.[10] The detectable effects appear only in $A_{YY}(51°)$ and $A_{YY}(65°)$ as shown in Fig. 8, which displays the excitation functions. The detailed shapes of the energy dependence are sensitive to the model-dependent background phases. Shifts in the curves may be expected from variations in the model. No other *pp* experimental quantity showed measurable structures at these energies.

The observable effects of both the $^3S_1$ and $^1S_0$ resonances in the *np* system are found to be more rich. The most significant structures with characteristic signature appear for $d\sigma/d\Omega(58°)$, $D(56°)$, $A_{XX}(50°)$, $A_{XX}(70°)$, $A_{ZZ}(124°)$, and $R'(170°)$. The excitation functions of these quantities are shown in Fig. 9. These measurable bumps have the predicted six-quark signatures of width and isospin splitting for identification. Although closer to

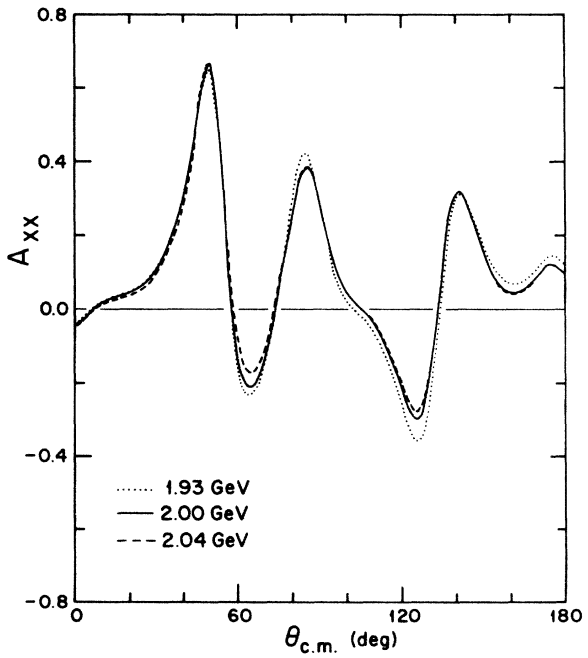

FIG. 7. The angular distributions of the *np* spin correlation observable A_{XX} for $T_L = 1.93$, 2.00, and 2.04 GeV. The $^1S_0$ model near resonance is that of Fig. 2.

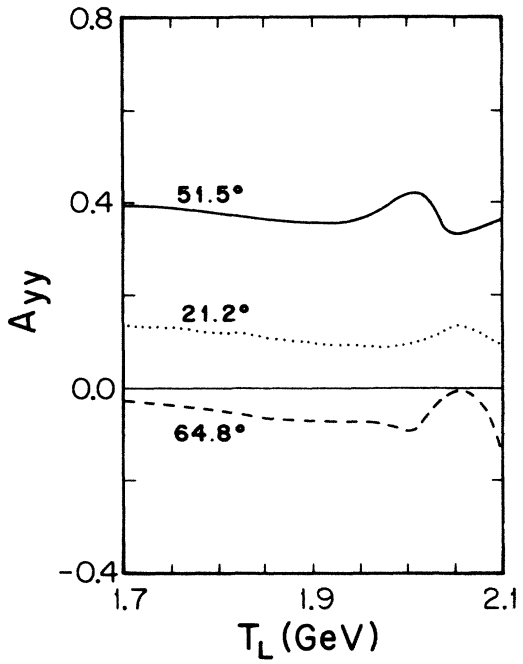

FIG. 8. The *pp* spin correlation observable A_{YY} as a function of laboratory energy at several sensitive angles, for the $^1S_0$ model of Fig. 2.

the observable limit, several choices are possible among other observables, for instance $A_{YY}(130°)$, $D(92°)$, $D_t(44°)$, $A_{ZX}(136°)$, $R(146°)$, and $R'(134°)$, plotted in Fig. 10. The changes in slope at the resonance positions in the remaining quantities P, A, and A' were more gentle and therefore not measurable.

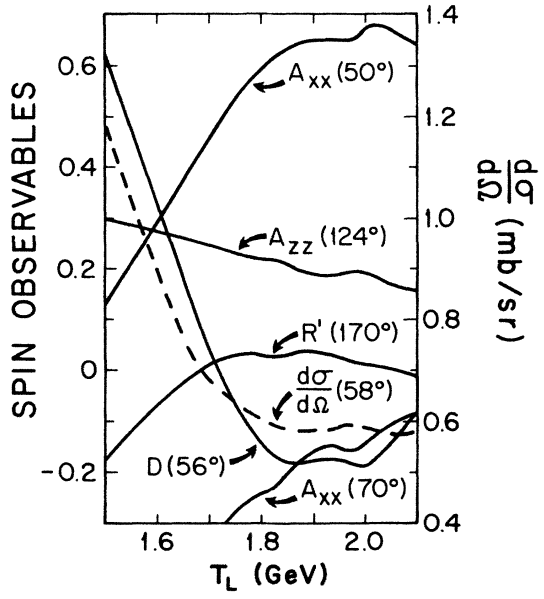

FIG. 9. Energy dependences of several *np* polarization observables in the vicinity of both the $^3S_1$ and $^1S_0$ resonances, for models shown in Figs. 2–4. This sample of the quantities $d\sigma/d\Omega$, D, A_{XX}, A_{ZZ}, and R' is characteristic of the q^6 signatures discussed in the text.

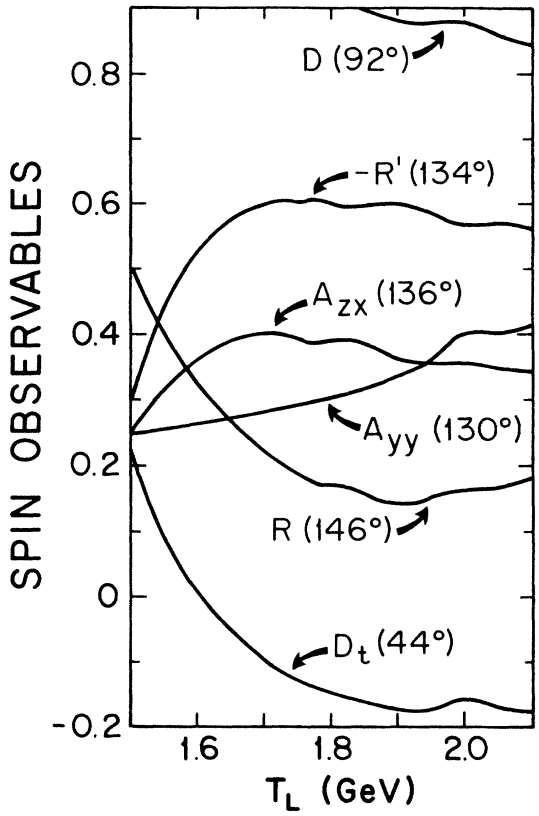

FIG. 10. Choices among the subset of *np* polarization observables A_{YY}, D, D_t, A_{ZX}, R, and $-R'$ whose excitation functions feature the six-quark resonances, but with smaller amplitudes than the observables of Fig. 9.

A change in the model extrapolation beyond $T_L = 800$ MeV of the $^3S_1$-$^3D_1$ phases may increase or decrease the size of the phase-shift structure at resonance and consequently the size of the observable structures. A model which takes into account production channels with threshold higher than the $\Delta\Delta$ system will lower the value of the effective f in the two-nucleon channels at higher energies and thus increase the coupling to the interior. To illustrate, we use a variation of the NN-$\Delta\Delta$-NN^* model that has a smaller effective f in the resonance region at the expense of a poor fit to ϵ_1 for $T_L \leq 800$ MeV. The resulting phase parameters are shown in Figs. 3 and 4 (dashed curves). It is likely that a model including higher-mass thresholds could simultaneously reproduce the phase shifts at low energy and have a lower effective f. At the $^3S_1$ resonance the effective f of the background to the $NN(^3S_1)$ channel is 33.3 for the first (good fit) case and 11.4 for the second case, in the approximation of Eq. (6). Figure 11 shows that several excitation curves of *np* experiments which have no, or little, structure for the first case, have very large structures for the second case. It is therefore possible that the observable effects may be much more marked than indicated in Figs. 8–10. However, they may also be smaller if features of the model, other than the addition of higher mass thresholds, are changed.

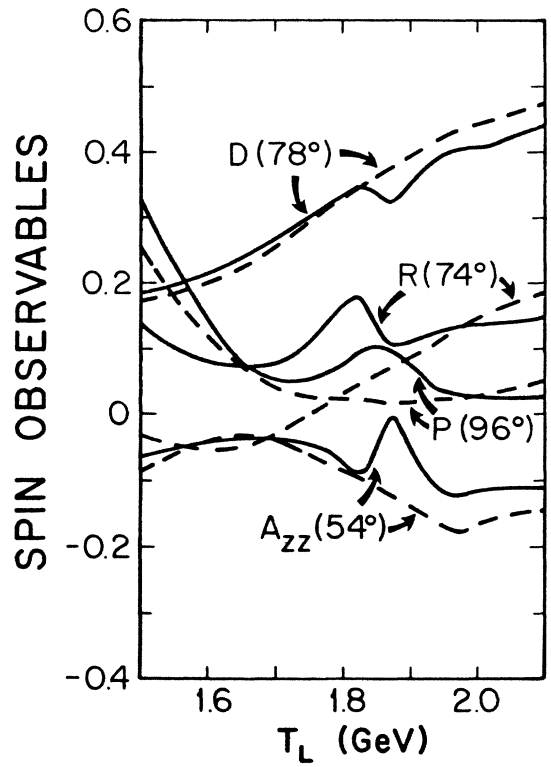

FIG. 11. Selective comparison between observable effects in a few *np* polarization experiments, P, D, A_{ZZ}, and R, coming from two different $^3S_1$-$^3D_1$ models. The dashed curves correspond to the results from the models of Figs. 2–4, used in this paper, and where the effective f of the background at the $^3S_1$ resonance is big (see text). The solid curves represent the results from the model of Ref. 12 (dashed curves of Figs. 3 and 4) for which ϵ_1 has a wrong sign. The point here, however, is the large increase in resonance effects due to the small effective f of the background at the $^3S_1$ resonance.

V. CONCLUSIONS

We have shown, using R-matrix theory, that the MIT (Ref. 13) and Carlson-Hanson-Peterson[14] bag models are inconsistent with the detailed nucleon-nucleon $^1S_0$ and $^3S_1$-$^3D_1$ scattering data for $T_L \leq 800$ MeV. The cloudy bag model[18] is consistent, or nearly consistent, with this data, and the fit then predicts inelastic six-quark resonances in the $^1S_0$ wave at $T_L = 2.00$ GeV and in the $^3S_1$-$^3D_1$ wave at $T_L = 1.82$ GeV. It is shown that the ~ 50 MeV widths of these dibaryons, the 70 MeV mass splitting of the $^1S_0$ resonance from the $^3S_1$-$^3D_1$ resonance, and the strong variation of the two-Δ production are insensitive to the specific QCD model used and are signatures of the free six-quark content of these systems.

The absolute mass of these dibaryons is sensitive to the model. Nevertheless, consideration of the range of six-quark models (from the MIT bag model which is too expanded to that of Ref. 14 which is collapsed) and the bound of the Wigner causality condition strongly indicate that these S-state resonances should be present at masses of less than 3.5 GeV. Consequently, they may be observable with existing high-intensity polarized proton beam accelerators.

Extrapolation of the partial-wave phase shifts to the six-quark resonance region, using reasonable coupled-channel models, has been used to investigate the size of observable consequences. While only one *pp* spin observable, A_{YY}, has a measurable structure at the $^1S_0$ resonance, several *np* observables show measurable structures for both the $^1S_0$ and $^3S_1$-$^3D_1$ resonances. In particular, excitation functions at indicated angles for $d\sigma/d\Omega$, D, A_{XX}, A_{ZZ} and R' have the largest predicted effects, while measurable effects also appear in A_{YY}, D_t, A_{ZX}, and R.

A program of *np* scattering, in addition to *pp* scattering, at laboratory energies above 1 GeV is of importance to the search for these structures. In addition, two-pion production experiments could directly explore coupling to the $\Delta\Delta$ content of the six-quark states. The resulting information would enable the determination of QCD characteristics not easily examined by very high-momentum-transfer reactions or through study of the single-hadron spectrum.

Because of the sensitivity of the magnitude of the observable consequences to the model phase-shift extrapolations, we are undertaking more refined model determinations.[27] More realistic models[26] and the growing amount of data for $T_L > 800$ MeV will be taken into account. Pion-production data will be a further control.

This paper has examined details of the lowest six-quark resonances, usually called dibaryons, in the nucleon-nucleon system. But the phenomenon of exotic quark-gluon states may appear in a wide variety of two-hadron reactions. Each case can elucidate a different aspect of the quark-gluon dynamics. The following is a brief review of the possibilities.

Other low-lying NN channels will have resonances split from the $^1S_0$ and $^3S_1$ by model insensitive color-magnetic effects. The $^5S_2(\Delta\Delta)$ configuration [connected to the $^5S_2(N\Delta)$ and $^1D_2(NN)$ via long-range interactions] and the $^7S_3(\Delta\Delta)$ configuration [connected to $^3D_3(NN)$] are expected to be about 110 MeV above the $^1S_0$ in mass. Their widths are expected to be narrow because they are also 80% hidden color and have an angular momentum barrier to the NN channel.

When strange quarks are included in the $^1S_{1/2}$ quark states then the N-Λ splitting determines the strange-quark mass and the resulting resonance splitting. Because $r_0 < r_{eq}$ these states are expected to be 100 MeV or more above the predictions of the MIT bag model. We therefore expect the $H(\Lambda\Lambda)$ to be in the continuum. Exploring these resonances requires Λ, Σ, and Ξ beams.

Orbital excitations of the quarks will lead to states with about 0.5 GeV more mass than the lower orbital excitation. Collective effects may decrease this splitting.

In the meson-meson and meson-baryon sectors, the choice of r_0 slightly smaller than r_{eq} can improve on the results of Refs. 5 and 6. In the nucleon-antinucleon sector, passage through $q^2\bar{q}^2$ configurations may lead to narrow resonances because of the annihilation and creation of quark pairs, but mixing with $q^3\bar{q}^3$ configurations must be considered.

If gluons are added to the configurations, one may ex-

pect structures at steps of 100–200 MeV for each gluon.

A primary polarized proton beam of variable energy in the 1–10-GeV range with its associated secondary neutron, pion, and kaon beams will enable detailed, precise measurements of most of these effects. A cooled antiproton beam of a few GeV energy is also needed. An electron accelerator of a few GeV energy will enable observation of the form factors of those states that can be excited from a deuteron or other light nucleus.

In the above applications of the R-matrix method we have assumed that asymptotic freedom is adequate inside the boundary, and that hadronification is complete outside. One may contemplate the use of more exact interior and exterior Hamiltonians in future work. It is possible that, with the advantage of restricted spatial dimensions, a lattice QCD calculation for the interior states would be feasible for $r_0 \lesssim 1.5$ fm, in spite of the nonperiodic boundary conditions. This would justify a larger r_0 than consistant with interior asymptotic freedom, improving the accuracy of a hadronic exterior. On the other hand, one could take into account color leakage to the exterior (which may occur significantly for our smaller values of r_0) by coupling colored pairs to the hadronic channels in the exterior. The expected linear confining potentials in the colored pair channels will restrict them to small distances beyond r_0 and reduce their perturbation of the hadronic channels. Although we believe that our present approximations give an adequate indication of the character of the multiquark resonances, such refinements may be justified for precise comparison with experimental results.

ACKNOWLEDGMENTS

One of us (P.L.F.) is grateful for the support provided by the Natural Sciences and Engineering Research Council of Canada. The other author (E.L.L.) benefited from the hospitality and facilities of Los Alamos National Laboratory, University of Paris VI, University College, London, University of California at Los Angeles, and the University of Washington, Seattle, at various times during the preparation of this article.

[1]M. Creutz, Phys. Rev. Lett. **45**, 313 (1980).

[2]C. G. Callen, R. F. Dashen, and D. J. Gross, Phys. Rev. Lett. **44**, 435 (1980).

[3]M. Harvey, Nucl. Phys. **A352**, 301 (1980); M. Oka and K. Yazaki, Prog. Theor. Phys. **66**, 556, 572 (1981); A. Faessler and F. Fernandez, Phys. Lett. **124B**, 145 (1983); K. Maltman and N. Isgur, Phys. Rev. Lett. **50**, 1827 (1983).

[4]A. M. Badalyan and Yu A. Simonov, Yad. Fiz. **36**, 1479 (1982) [Sov. J. Nucl. Phys. **36**, 860 (1982)]; Y. E. Kim and M. Orlowski, Phys. Lett. **140B**, 275 (1984).

[5]R. L. Jaffe and F. E. Low, Phys. Rev. D **19**, 2105 (1979).

[6]C. Roiesnel, Phys. Rev. D **20**, 1646 (1979).

[7]P. J. Mulders, Phys. Rev. D **26**, 3039 (1982); R. P. Bickerstaff, Philos. Trans. R. Soc. London **A309**, 611 (1983).

[8]E. L. Lomon, in *Hadron Substructure in Nuclear Physics*, proceedings of the Workshop, Indiana University, 1983, edited by W. Y. P. Hwang and M. H. Macfarlane (AIP Conf. Proc. No. 110) (AIP, New York, 1984), p. 117. Earlier references are cited in this paper.

[9]E. L. Lomon, in *Particles and Nuclei*, proceedings of the Tenth International Conference, Heidelberg, 1984, edited by B. Povh and G. zu Pulitz [Nucl. Phys. **A434**, 139c (1985)].

[10]E. L. Lomon, in *Proceedings of the 6th International Symposium on High Energy Spin Physics, Marseille, 1984*, edited by J. Soffer [J. Phys. (Paris) Colloq. **46**, C2-329 (1985)].

[11]E. P. Wigner and L. Eisenbud, Phys. Rev. **72**, 29 (1947); A. M. Lane and R. G. Thomas, Rev. Mod. Phys. **30**, 257 (1958).

[12]H. Feshbach and E. L. Lomon, Ann. Phys. (N.Y.) **29**, 19 (1964).

[13]T. DeGrand *et al.*, Phys. Rev. D **12**, 2060 (1975).

[14]C. E. Carlson, T. H. Hansson, and C. Peterson, Phys. Rev. D **27**, 1556 (1983).

[15]E. L. Lomon and H. Feshbach, Ann. Phys. (N.Y.) **48**, 94 (1968).

[16]E. L. Lomon, Phys. Rev. D **26**, 576 (1982).

[17]E. L. Lomon, Phys. Rev. D **31**, 1746 (1985).

[18]P. J. Mulders and A. W. Thomas, J. Phys. G **9**, 1159 (1983).

[19]M. Lacombe *et al.*, Phys. Rev. C **21**, 861 (1980).

[20]M. Lacombe *et al.*, Phys. Rev. D **12**, 1495 (1975).

[21]R. Machleidt, Physics (N.Y.) **197**, 352 (1984).

[22]E. L. Lomon, Phys. Rev. D **1**, 549 (1970).

[23]P. J. Mulders, Phys. Rev. D **28**, 4431 (1983); R. L. Jaffe and M. Shatz, Caltech Report No. CALT-68-775, 1981 (unpublished).

[24]P. Sitarski, P. Blunden, and E. L. Lomon (in preparation).

[25]R. A. Arndt *et al.*, Phys. Rev. D **28**, 97 (1983).

[26]P. González and E. L. Lomon, Phys. Rev. D **34**, 1351 (1986).

[27]P. González, P. LaFrance, and E. L. Lomon, MIT Report No. CTP 1383, 1986 (unpublished).

[28]P. LaFrance and P. Winternitz, Phys. Rev. D **27**, 112 (1983).